OXFORD

SOT | Society of Toxicology
www.toxsci.oxfordjournals.org

TOXICOLOGICAL SCIENCES, 143(2), 2015, 482–498

doi: 10.1093/toxsci/kfu249
Advance Access Publication Date: January 8, 2015

Elevated Adult Neurogenesis in Brain Subventricular Zone Following *In vivo* Manganese Exposure: Roles of Copper and DMT1

Sherleen Fu, Stefanie O'Neal, Lan Hong, Wendy Jiang, and Wei Zheng[1]

School of Health Sciences, Purdue University, West Lafayette, Indiana 47907

[1]To whom correspondence should be addressed at School of Health Sciences, Purdue University, 550 Stadium Mall Drive, Room 1169, West Lafayette, IN 47907. Fax: (765) 496-1377. E-mail: wzheng@purdue.edu.

ABSTRACT

The brain subventricular zone (SVZ) is a source of neural precursor cells; these cells travel along the rostral migratory stream (RMS) to destination areas in the process of adult neurogenesis. Recent x-ray fluorescence (XRF) studies reveal an extensive accumulation of copper (Cu) in the SVZ. Earlier human and animal studies also suggest an altered Cu homeostasis after manganese (Mn) exposure. This study was designed to test the hypothesis that Mn exposure by acting on the divalent metal transporter-1 (DMT1) altered Cu levels in SVZ and RMS, thereby affecting adult neurogenesis. Adult rats received intraperitoneal (i.p.) injections of 6 mg Mn/kg as $MnCl_2$ once daily for 4 weeks with concomitant injections of bromodeoxyuridine (BrdU) for 5 days in the last week. In control rats, Cu levels were significantly higher in the SVZ than other brain regions examined. Mn exposure significantly reduced Cu concentrations in the SVZ ($P < 0.01$). Immunohistochemical data showed that *in vivo* Mn exposure significantly increased numbers of BrdU(+) cells, which were accompanied with increased GFAP(+) astrocytic stem cells and DCX(+) neuroblasts in SVZ and RMS. Quantitative RT-PCR and Western blot confirmed the increased expression of DMT1 in SVZ following *in vivo* Mn exposure, which contributed to Mn accumulation in the neurogenesis pathway. Taken together, these results indicate a clear disruptive effect of Mn on adult neurogenesis; the effect appears due partly to Mn induction of DMT1 and its interference with cellular Cu regulation in SVZ and RMS. The future research directions based on these observations are also discussed.

Key words: copper; manganese; subventricular zone; rostral migratory stream; divalent metal transporter-1; adult neurogenesis

Copper (Cu), for its readily interchangeable oxidation state between Cu^{1+} and Cu^{2+}, is vital to normal biological functions by acting as a cofactor for a host of enzymes that catalyze a wide range of cellular biochemical reactions (Lorraine *et al.*, 2011; Turski and Thiele, 2009; Uriu-Adams *et al.*, 2010). In the rodent brain, Cu preferentially accumulates in striatum (STR), frontal cortex (FC), hippocampus (HP), and cerebellum (Choi and Zheng, 2009; Zheng *et al.*, 2009). Functionally, Cu ions participate in neurotransmitter metabolism and regulate synaptic activities requiring cuproenzymes such as dopamine-β-monooxygenase, cytochrome C oxidase, lysyl oxidase, superoxide dismutase, and tyrosinase (Joseph and Bruce, 2001; Skjorringe *et al.*, 2012; Takahashi *et al.*, 2002). Free, unbound Cu ions can readily interact with oxygen to initiate cascades of biochemical reactions leading to the production of free radicals and increased oxidative stress (Deibel *et al.*, 1996; Turski and Thiele, 2009; Zheng and Monnot, 2012). Cumulative evidence suggests that an imbalanced Cu homeostasis in the brain, either excess or deficient, contributes to the pathogenesis of neurodegenerative disorders such as idiopathic Parkinson's disease, Alzheimer's disease, familial amyotrophic lateral sclerosis, prion disease, and the genetic disorders Wilson's disease and Menkes' disease (Barnham and Bush, 2008; Gaggelli *et al.*, 2006; Matés *et al.*, 2010; Zheng and Monnot, 2012). Thus, a stable Cu homeostasis in the central nervous system is essential to normal brain function.

Our recent works using synchrotron-based x-ray fluorescence (XRF) microscopy demonstrate that the Cu concentration in rat subventricular zone (SVZ) is about 20–30 times higher than that in other brain regions (Pushkar *et al.*, 2013). This finding is in good agreement with reports by other investigators (Matusch *et al.*, 2010; Pushie *et al.*, 2011). The SVZ is known to play a significant role in neurogenesis in adult brain (Curtis *et al.*, 2007; Ghashghaei *et al.*, 2007; Lledo *et al.*, 2006). Located alongside the wall of brain lateral ventricles, the SVZ serves as a source of neural stem cells in the process of adult neurogenesis. There are 4 major cell types in the SVZ, ie, (1) ependymal cells in immediate contact with the cerebrospinal fluid (CSF) that is largely secreted by the choroid plexus in brain ventricles, (2) β-tubulin or doublecortin (DCX) positive type-A migratory neuroblasts, (3) glial fibrillary acid protein (GFAP)-positive type-B astrocytic stem cells (ASCs), and (4) nestin-positive type-C transit amplifying cells (Doetsch *et al.*, 1997). Actively differentiated neuroblasts possess a unique ability to migrate from the SVZ origin, via the rostral migratory stream (RMS), to the olfactory bulb (Curtis *et al.*, 2007; Doetsch *et al.*, 1997; Imura *et al.*, 2006; Lois *et al.*, 1996). On the migratory path, these precursor cells may further divide and differentiate in adjacent brain regions to provide renewed neurons and therefore to compensate the loss of neurons due to neurodegenerative injury (Ghashghaei *et al.*, 2007; Lledo *et al.*, 2006; Martino and Pluchino, 2006). Reports in literature have suggested that the neuronal repair mechanism happens in brains of those suffering from Parkinson's disease or Alzheimer's disease (Curtis *et al.*, 2007; Martino and Pluchino, 2006). Limited studies have also suggested a role of Cu in regulating embryonic stem cell differentiation (El Meskini *et al.*, 2007; Haremaki *et al.*, 2007; Niciu *et al.*, 2007). However, knowledge on whether and how Cu is involved in regulation of neural differentiation in brain, particularly in the SVZ and RMS, remain elusive.

Maintaining a stable Cu homeostasis in the brain requires membrane-associated Cu transporters such as divalent metal transporter-1 (DMT1), copper transporter-1 (CTR1), and Cu exporter ATPases, and a subset of intracellular Cu chaperones such as antioxidant protein-1, cytochrome oxidase enzyme complex, and Cu chaperone for super oxide dismutase (Harris, 2001). DMT1 is a proton-driven transporter capable of nonselective transport of divalent metals including manganese (Mn), Cu, iron (Fe), cobalt, zinc (Zn), cadmium, and lead (Gruenheid *et al.*, 1995; Gunshin *et al.*, 1997). Previous studies from this laboratory have shown that DMT1 is required for transporting Fe and Cu across the blood-brain barrier and blood-CSF barrier (Wang *et al.*, 2006; Zheng and Monnot, 2012). In the study of Cu transport by the choroid plexus, Monnot *et al.* (2012) reported a significant increase in mRNA levels of DMT1, but not CTR1, in the Fe-deficient state, suggesting the importance of DMT1 in cellular Cu regulation. Burdo *et al.* (2001) found that DMT1 was expressed prominently in ependymal cells of the third ventricle of rat brain. These observations raise the question as to whether DMT1 participates in regulating Cu accumulation in SVZ cells lining the lateral ventricles.

Studies by this laboratory reveal that chronic exposure to Mn in adult rat results in a significant increase of Cu concentrations in the CSF, choroid plexus, STR, HP, and FC (Zheng *et al.*, 2009). Since the choroid plexuses in brain ventricles are adjacent to the SVZ, it became interesting to learn if Mn intoxication altered the Cu status in the SVZ in the same fashion as it does in the choroid plexus. Noticeably, during development, Mn exposure in mice has been shown to induce the aberration in neurogenesis and neuronal migration in hippocampal dentate gyrus; the effect could continue during postnatal life into adulthood (Wang *et al.*, 2012). Since the SVZ supports neurogenesis and neural repair, a distorted Cu homeostasis in this area by Mn exposure may interfere with the critical events necessary for neural differentiation and migration, which may lead to the disordered neurogenesis in Mn-induced neurotoxicity.

The purposes of this study were to (1) determine Cu concentrations in brain regions (SVZ, STR, and HP) as affected by Mn exposure by using atomic absorption spectroscopy (AAS); (2) examine whether Mn exposure altered neurogenesis activity in SVZ and RMS; (3) investigate the expression of DMT1 in the SVZ and RMS and examine whether Mn exposure affected the expression level of DMT1 in these regions. The results of this study provide evidence of Mn interaction with neuronal repair processes and likely create a new avenue in Mn neurotoxicological research.

MATERIALS AND METHODS

Materials. Chemical reagents were purchased from the following sources: Rabbit anti-rat DMT1 antibody was obtained from Alpha Diagnostic (San Antonio, California); mouse monoclonal anti-bromodeoxyuridine (BrdU) antibody from Santa Cruz Biotechnology (Dallas, Texas); ProLong Gold anti-fade reagent, Alexa Fluor 488 goat anti-rabbit IgG (H + L) antibody, Alexa Fluor 555 goat anti-mouse IgG (H + L) antibody, and Alexa Fluor 633 goat anti-chicken IgG (H + L) antibody from Life Technologies (Carlsbad, California); mouse anti-GFAP from millipore (Billerica, Massachusetts); rabbit polyclonal anti-DCX antibody and chicken polyclonal anti-GFAP antibody from Abcam (Cambridge, Massachusetts); manganese chloride tetra-hydrate ($MnCl_2$) from Fisher scientific (Pittsburgh, Pennsylvania); Protease Inhibitor Cocktail from Calbiochem (San Diego, California); Tris base, glycine, sodium dodecyl sulfate (SDS), 2 × Laemmli sample buffer, triton X-100, cDNA synthesis kit, iTaq Universal SYBR Green Supermix, clarity Western enhanced chemiluminescence (ECL) substrate from Biorad (Hercules, California); mouse BrdU, mouse anti-β-actin, 2-mercaptoethanol, phenylmethyl-sulfonylfluoride, polyacrylamide, and tetramethyl-ethylenediamine from Sigma Chemicals (St Louis, Missouri); ECL anti-mouse IgG and anti-rabbit IgG (horseradish peroxidase linked whole antibodies, from sheep) from GE Healthcare (Piscataway, New Jersey); paraformaldehyde (PFA) from ACROS Organics (New Jersey); bovine serum albumin (BSA) from AMRESCO (Solon, Ohio); ultrapure nitric acid (HNO_3) from Mallinckrodt (St Louis, Missouri). All reagents were of analytical grade, high-performance liquid chromatography (HPLC) grade, or the best available pharmaceutical grade.

Animals and Mn exposure. Male Sprague Dawley rats were purchased from Harlan Sprague Dawley Inc (Indianapolis, Indiana). At the time of use, rats were 10 weeks old weighing 220–250 g. Upon arrival, rats were housed in a temperature-controlled room under a 12-h light/12-h dark cycle and allowed to acclimate for 1 week prior to experimentation. They had free access to deionized water and pellet Purina semi-purified rat chow (Purinal Mills Test Diest, 5755C. Purina Mills, Richmond, Inc). The study was conducted in compliance with standard animal use practices and approved by the Animal Care and Use Committee of Purdue University.

$MnCl_2{\cdot}4H_2O$ dissolved in sterile saline was administrated to rats by i.p. injection with 1 ml/kg body weight at the dose of 6 mg Mn/kg, once daily, 5 days/week for 4 consecutive weeks. The daily equivalent volume of sterile saline was given to the

animals in the control group. Twenty-four hours after the last injection, rats were anesthetized with ketamine/xylazine (75:10 mg/kg, 1 mg/kg i.p.). Fresh brain tissues, ie, SVZ, STR, and HP, were collected for measurement of Mn and Cu levels using AAS, and to determine the expression levels of DMT1, GFAP, Nestin, and DCX by using Western blot or qPCR. Samples were freshly analyzed or stored at −80°C for later analysis.

Determination of Mn and Cu concentrations by AAS. Brain samples were digested with concentrated ultrapure HNO3 in a MARSXpress microwave-accelerated reaction system. SVZ samples were digested overnight with HNO3 in the oven at 55°C. An Agilent Technologies 200 Series SpectrAA with a GTA 120 graphite tube atomizer was used to quantify Mn and Cu concentrations. Digested samples were diluted by 50, 500, or 1000 times with 1.0% (vol/vol) HNO_3 in order to keep the reading within the concentration range of standard curves. Ranges of calibration standards for Mn and Cu were 0–5 μg/l and 0–25 μg/l, respectively. Detection limits for Mn and Cu were 0.09 ng/ml and 0.9 ng/ml, respectively, of the assay solution. Intra-day precision of the method for Mn and Cu was 2.9% and 1.6%, respectively, and the inter-day precision was 3.3% and 3.7%, respectively (Zheng *et al.*, 1998, 1999, 2009).

Tissue preparation. To study the effect of Mn exposure on neurogenesis proliferation in the SVZ and RMS, groups of rats (3 controls and 3 Mn-exposed rats) concomitantly received i.p. injections of 50 mg/kg of BrdU twice daily for 5 days during the last week of Mn administration. Rats were anesthetized 12 h after the last BrdU treatment (24 h after the last Mn injection) using ketamine/xylazine (75:10 mg/kg, 1 mg/kg i.p.). Brains were fixed by heart perfusion with 4% PFA in phosphate-buffered saline (PBS). Brains were then removed from the skull and post-fixed in 4% PFA for 24 h followed by dehydration process in 30% sucrose for 7 days. Brains were then bisected mid-sagittally and sectioned with a microtome to collect brain sections in 30 μm thickness: one hemisphere was sectioned sagittally (Lateral 1.90 mm) and the other hemisphere was sectioned coronally (Bregma 0.20 mm).

Immunohistochemistry staining. The combinations of immunohistochemistry (IHC) staining were conducted as followed: (1) to examine whether DMT1 was expressed in neural proliferating cells, brain sections were double-stained with mouse anti-BrdU (1:400) and rabbit anti-DMT1 primary antibodies (1:400) at 4°C, overnight, followed by incubation with Alexa Fluor 555 goat anti-mouse IgG (H + L) antibody (1:500) and Alexa Fluor 488 goat anti-rabbit IgG (H + L) antibody (1:500) at room temperature (RT), for 1.5 h; (2) to identify whether the BrdU(+) cells were also positive with GFAP (an ASCs marker) or DCX (a neuroblast marker), brain sections were triple-labeled with mouse anti-BrdU primary antibody (1:400), chicken anti-GFAP primary antibodies (1:1000) and rabbit anti-DCX primary antibodies (1:1000) at 4°C, overnight, followed by treatment with Alexa Fluor 555 goat anti-mouse IgG (H + L) antibody (1:500), Alexa Fluor 633 goat anti-chicken IgG (H + L) (1:1000), and Alexa Fluor 488 goat anti-rabbit IgG (H + L) antibody (1:1000) at RT, for 1.5 h; and (3) to study whether DMT1(+) cells were also expressed GFAP, brain sections were incubated with mouse anti-GFAP primary antibody (1:1000) and rabbit anti-DMT1 primary antibodies (1:400) at 4°C, overnight, followed by incubation with Alexa Fluor 555 goat anti-mouse IgG (H + L) antibody (1:1000) and Alexa Fluor 488 goat anti-rabbit IgG (H + L) antibody (1:500) at RT, for 1.5 h.

Free-floating brain sections were stored in cryoprotectant solution at −20°C before IHC staining. About 6–10 floating sections from each animal were sorted and washed in PBS (3 × 10 min), followed by blocking the sections in 2 N hydrogen chloride at RT for 2 h to denature DNA. After rinsed with PBS (3 × 10 min), sections were blocked in 1% BSA containing 0.5% Triton X-100 and 10% normal goat serum at RT for 1 h and then treated with various antibody combinations as described above. Sections were washed with PBS (3 × 10 min) between blockings of different antibodies and then mounted to slides with ProLong Gold anti-fade reagent and allowed to air dry overnight at RT before examination using a confocal microscope (C1-plus, Nikon). In order to obtain precise and comparable image data between 2 groups, regions from the control and Mn-exposed brain sections were carefully matched according to the bregma prior to IHC staining analysis. Images were analyzed and quantified using the software of NIS Elements BR from Nikon. Confocal images (×100) taken from coronal and sagittal sections were used to quantify both DMT1 and BrdU fluorescent intensities for SVZ and RMS. The locations of BrdU(+) proliferating cells in the SVZ and RMS were manually selected as the region of interest (ROI) for quantitation. The fluorescent intensities of DMT1 within the selected BrdU-ROI were then quantitated. The intensity quantification data from 3 to 6 sections of each animal were collected; the average intensity of these intensity data of the same animal was then calculated and processed for the statistical analysis to compare the difference between control and Mn-exposed groups.

qPCR and Western blot. The transcription levels of mRNA encoding *Dmt1*, *Gfap*, *Nestin* (a specific marker for neuronal precursor cells of SVZ), and *Dcx* were quantified using qPCR. Total RNA was isolated from control and Mn-exposed rat SVZ tissues by using TRIzol reagent following the manufacturer's directions. An aliquot of RNA (1 μg) was reverse-transcribed into cDNA using the BioRad iScript cDNA synthesis kit. The iTaq Universal SYBR Green Supermix was used for qPCR analyses. The amplification was run in the CFX Connect Real-Time PCR Detection system with an initial 3 min denaturation at 95°C, the amplification program was followed by 40 cycles of 30 s denaturation at 95°C, 10 s gradient from 55°C to 65°C and 30 s extension at 72°C. A dissociation curve was used to verify that the majority of fluorescence detected could be attributed to the labeling of specific PCR products, and to verify the absence of primer dimers and sample contamination. Each qPCR reaction was run in triplicate. The relative mRNA expression ratios between groups were calculated using the delta-delta cycle time formulation. After confirming that the reference gene was not changed, the cycle time values of interested genes were normalized with that of the reference gene in the same sample, and then the relative ratio between control and treatment groups was calculated and expressed as relative increases by setting the control as 100%. The amplification efficiencies of target genes and the internal reference were examined by determining the variations of the cycle time with a series of control template dilutions.

The forward and reverse primers for *Dmt1*, *Gfap*, *Nestin*, *and Dcx* genes were designed using Primer Express 3.0 software. Primers sequences for rat *Dmt1* used in this study were: forward primer 5′-GAT TCC AGA CGA TGG TGC TT-3′ and reverse primer 5′-GTG AAG GCC CAG AGT TTA CG-3′ (GenBank Accession No. NM_013173.2); primers sequences for rat *Gfap* used in this study were: forward primer 5′-TAG CAT AAG TGG AGA GGG AA-3′ and reverse primer 5′-GGA TTC AGA GCC AAG TGT AA-3′ (GenBank Accession No. NM_017009.2); primers sequences for rat *Nestin*

TABLE 1. Brain Regional Concentrations of Mn and Cu with or without *in vivo* Subchronic Mn Exposure by AAS Quantification

Group	Mn Concentration (μg/g Tissue)			Cu Concentration (μg/g Tissue)		
	SVZ	STR	HP	SVZ	STR	HP
Ct	0.93 ± 0.31	0.99 ± 0.29	0.68 ± 0.22	17.8 ± 4.61	1.32 ± 0.27$^{\#\#}$	0.81 ± 0.12$^{\#\#}$
Mn-E	1.81 ± 0.30**	3.06 ± 0.39**	1.80 ± 0.29**	10.5 ± 1.20**	1.87 ± 0.33*	0.86 ± 0.08

Notes: Data represent mean ± SD, $n = 4$–6 (SVZ), $n = 8$–10 (STR and HP). $^{*}P < 0.05$, $^{**}P < 0.01$, when compared with the control; $^{\#\#}P < 0.01$, when compared with the control SVZ Cu level. SVZ, subventricular zone; STR, striatum; HP, hippocampus; Ct, control group; Mn-E, Mn-exposed group.

used in this study were: forward primer 5′-ATG AGG GGC AAA TCT GGG AA-3′ and reverse primer 5′-CCA GGT GGC CTT CTG TAG AA-3′ (GenBank Accession No. NM_012987.1); primers sequences for rat *Dcx* used in this study were: forward primer 5′-ACT GAA TGC TTA GGG GCC TT-3′ and reverse primer 5′-CTG ACT TGC CAC TCT CCT GA-3′ (GenBank Accession No. NM_053379.3). The rat β-actin (*Actb*) was used as an internal control, with the forward primer 5′-AGC CAT GTA CGT AGC CAT CC-3′ and the reverse primer 5′-CTC TCA GCT GTG GTG GTG AA-3′ (GenBank Accession No. NM_031144.3). All primers were obtained from Integrated DNA Technologies (Coralville, Iowa). Experimental conditions were optimized for annealing temperature, primer specificity, and amplification efficiency.

Total cellular proteins from control and Mn-treated SVZ tissues were extracted in a homogenization buffer containing 20mM Tris, pH 7.5, 5mM ethylene glycol tetraacetic acid (EGTA), 1% Triton X-100, 0.1% SDS, and protease inhibitor cocktail. Samples were sonicated, centrifuged (12 000 × g for 15 min) and quantified for protein concentration using a Bradford protein assay. A volume of protein samples were mixed and boiled in an equal volume of 2 × Laemmli sample buffer. Protein samples (100 μg protein/sample) were then loaded on the 12% Tris-glycine SDS-polyacrylamide gels, electrophoresed, and transferred to polyvinylene difluoride membranes which were then blocked with 5% dry milk in Tris-buffered saline with 0.1% Tween 20 and incubated overnight at 4°C with the polyclonal rabbit anti-DMT1 primary antibody (1:10 000). Following washes using Tris-buffered saline with 0.1% Tween 20 (3 × 10 min), membranes were stained with a horseradish-peroxidase-conjugated goat anti-rabbit IgG antibody (1:3000) at RT for 1 h, and then developed using the Biorad Clarity Western ECL Substrate and the BioRad Molecular Imager (ChemiDoc XRS + with Image Lab Software; Biorad). Beta-actin (42 kDa) was used as an internal control. The band intensity was further quantified using Image J and reported in relative optical density ratio.

Statistical analyses. All data are presented as mean ± SD. Statistical analyses of the differences between control and Mn-exposed groups were carried out by Student's *t* tests using IBM SPSS for Windows (version 21.0). The differences between two means were considered significant for $P \leq 0.05$.

RESULTS

Mn and Cu Levels in Different Rat Brain Regions

AAS analyses of brain tissues revealed that Mn concentrations in all selected brain regions of SVZ, STR, and HP were significantly increased following subchronic Mn exposure at 6 mg/kg ($P < 0.01$) (Table 1). The accumulation of Mn in the SVZ may indicate a potential disturbance on the homeostasis of Mn or other metals in this region where adult neurogenesis occurs.

Among control animals, the Cu concentration in the SVZ was about 6.7- and 22-fold higher than those in STR ($P < 0.01$) and HP ($P < 0.01$), respectively; the data confirm the previous synchrotron XRF observations (Matusch *et al.*, 2010; Pushie *et al.*, 2011; Pushkar *et al.*, 2013) that SVZ accumulates extraordinarily high Cu levels under physiological condition. In our previous studies (Fu *et al.*, 2014; Zheng *et al.*, 2009), the subchronic Mn exposure at 6 mg/kg (the same dose regimen used in this current study) results in significant increases of Cu levels in STR, HP, and motor cortex. Consistently, our AAS results also showed significant elevation in STR Cu level ($P < 0.05$), following *in vivo* Mn exposure (Table 1). Interestingly, the same exposure regimen at 6 mg/kg in this study did not increase, but rather reduced the Cu concentrations in the SVZ from 17.8 ± 4.61 (mean ± SD) to 10.5 ± 1.20 μg/g ($P < 0.01$) (Table 1). It appears likely that the reduction of Cu level in the SVZ may disrupt the microenvironment that requires the high level of Cu in this adult neurogenesis cradle.

Elevated Adult Neurogenesis in the SVZ and RMS Following In Vivo Subchronic Mn Exposure

Confocal images of coronal brain sections in Figure 1A demonstrated that BrdU was mainly concentrated along the external wall of lateral ventricles where the SVZ is located. In the sagittal brain sections, BrdU-positive cells clearly presented in the SVZ region and also extended into the RMS (Fig. 2A).

A higher accumulation of metals in a particular brain region could be due to a higher expression of metal transporting proteins in that region. In this study, we focused on DMT1, because it is known to mediate cellular Mn and Cu uptake in various cell types. IHC staining of brain sections demonstrated the presence of DMT1 along the SVZ and RMS regions in control animals (Figs. 1A and 2A). Noticeably, BrdU fluorescent signals were colocalized with those of DMT1 in neural precursor cells in both SVZ and RMS (Figs. 1B and 2B).

We hypothesized that Mn accumulation in SVZ may inhibit neurogenesis in SVZ and RMS. To test this hypothesis, groups of rats (3 control and 3 Mn-treated) received pulse injections with BrdU during the last week of Mn treatment. In contrary to our original hypothesis, significant increases in BrdU signals were observed in both SVZ and RMS (Figs. 1 and 2). By signal quantitation, the BrdU fluorescent intensity in coronal sections of the SVZ was increased by about 85% ($P < 0.01$) when compared with controls (Fig. 1C). There was about 60% increase in BrdU signals in RMS after Mn exposure ($P < 0.01$) (Fig. 2C). Along the RMS, Mn exposure appeared to form a more densely packed, chain-like structure than that of the control (Fig. 2B).

Interestingly, a significantly increased fluorescence of DMT1 was also observed in both SVZ and RMS regions in Mn-treated animals when compared with controls (Figs. 1 and 2). Quantification of DMT1 fluorescent signals in sagittal sections indicated about 69% ($P < 0.05$) and 110% ($P < 0.05$) increases in

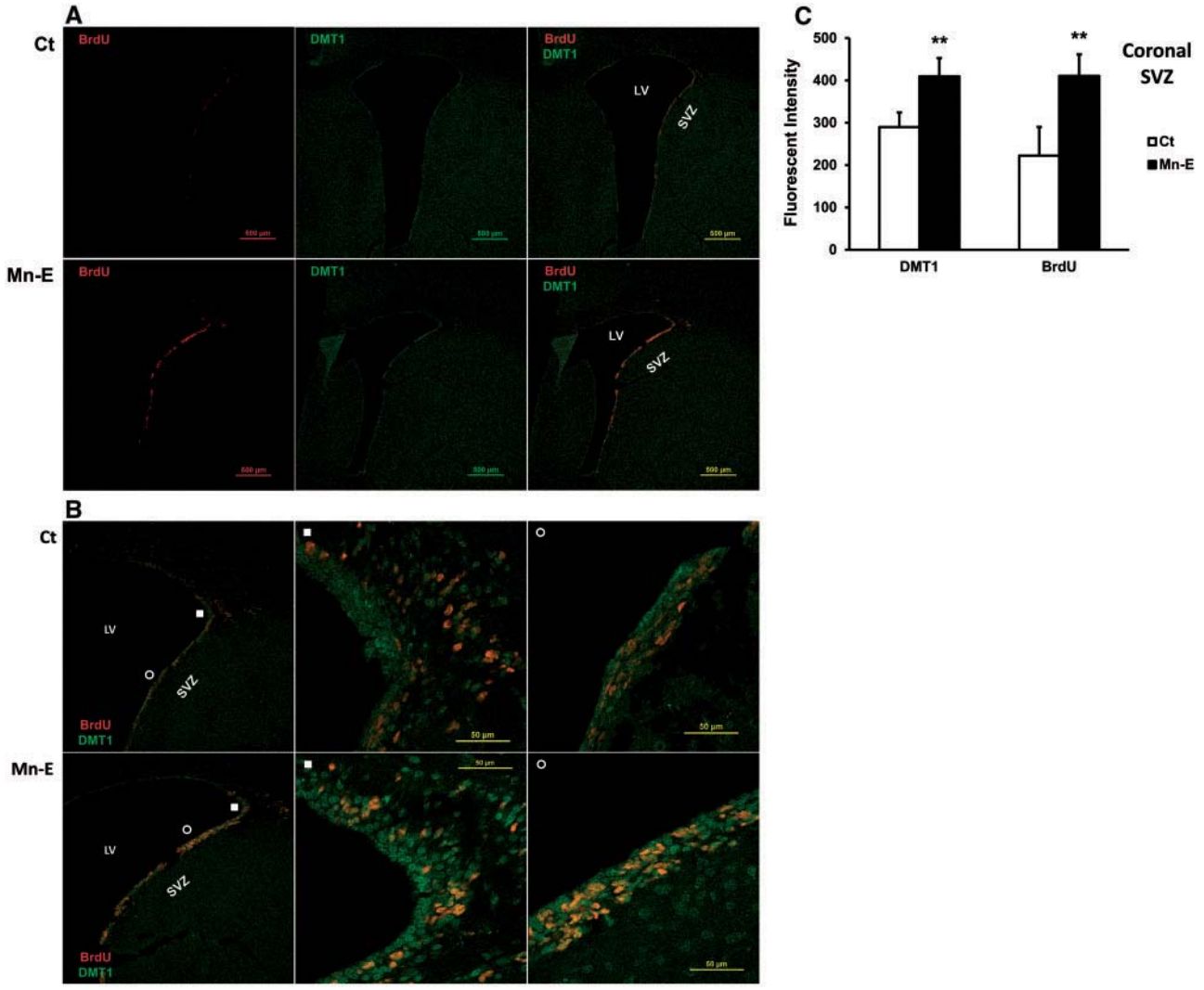

FIG. 1. IHC double-staining of BrdU and DMT1 in the SVZ by coronal sections. Rats received i.p. injection of 6 mg Mn/kg once daily, 5 days per week, for 4 weeks. BrdU was injected in the last 5 days. A, Typical coronal images at low magnification (×40) from control and Mn-exposed animals stained for BrdU (red) and DMT1 (green). Images were taken sequentially using the same imaging parameters. B, Typical coronal images at high magnifications (×100 or × 600). The symbols of white square and circle represent the approximate regions used to "zoom-in" the confocal images with ×600 in magnification. Additional confocal data on coronal sections from the same experiments ($n = 3$) are presented in Supplementary Figure 1. C, Quantification of the intensity of fluorescent signals by DMT and BrdU. Data represent mean ± SD, $n = 3$; $^{**}P < 0.01$, when compared with the control. Ct, control group; Mn-E, Mn-exposed group.

SVZ and RMS, respectively, when compared with controls (Fig. 2C). Additional imaging data can be found in Supplementary Figures 1 and 2.

Colocalization of BrdU(+) Proliferating Cells with ASCs and Neuroblasts in the SVZ and RMS

Increased BrdU(+) cells after Mn exposure raised the question as to whether the increased proliferation occurred in ASCs, neuroblasts, or both. β-Tubulin is a common marker for neuronal cells, but is not specific to newly derived neuroblast cells. Thus, we chose DCX to specifically label proliferating neuroblasts. We used GFAP to label ASCs (type B cells) and DCX to label neuroblasts (type A cells). Triple-staining with BrdU, GFAP, and DCX in coronal brain sections showed that BrdU(+) cells in the SVZ region were accompanied along with the distributions of GFAP(+) astrocyte cell bodies and DCX(+) neuroblasts, suggesting that both cell types were actively proliferating cells in the SVZ (Figs. 3A and 3B1). Confocal images from control rats in Figures 3C1 and 3D1 with higher magnification clearly revealed that the majority of BrdU-labeled nuclei were surrounded by the green DCX fluorescent signals, and only a small fraction of BrdU(+) cell bodies were surrounded by the blue GFAP fluorescent signals, indicating that under the physical condition the BrdU(+) cell proliferation was mainly the DCX(+) neuroblasts in the SVZ region. In Mn-exposed brain sections (Figs. 3B2, 3C2, and 3D2), more abundant BrdU-, DCX-, and GFAP-labeled cell bodies were observed when compared with control brain sections in Figures 3B1, 3C1, and 3D1.

Double-staining with BrdU and GFAP in the RMS showed that the spatial distribution of GFAP(+) astrocytes along the RMS constructed a sheath-like tube network surrounding the RMS with a proposed function to escort the migrating neuroblasts (Supplementary Figs. 1A–D). Noticeably, these GFAP(+) cells in the RMS may represent dividing astrocytes along the RMS rather than GFAP(+) type B neuroprogenitors migrating from the SVZ. Double-staining with BrdU and DCX in the same

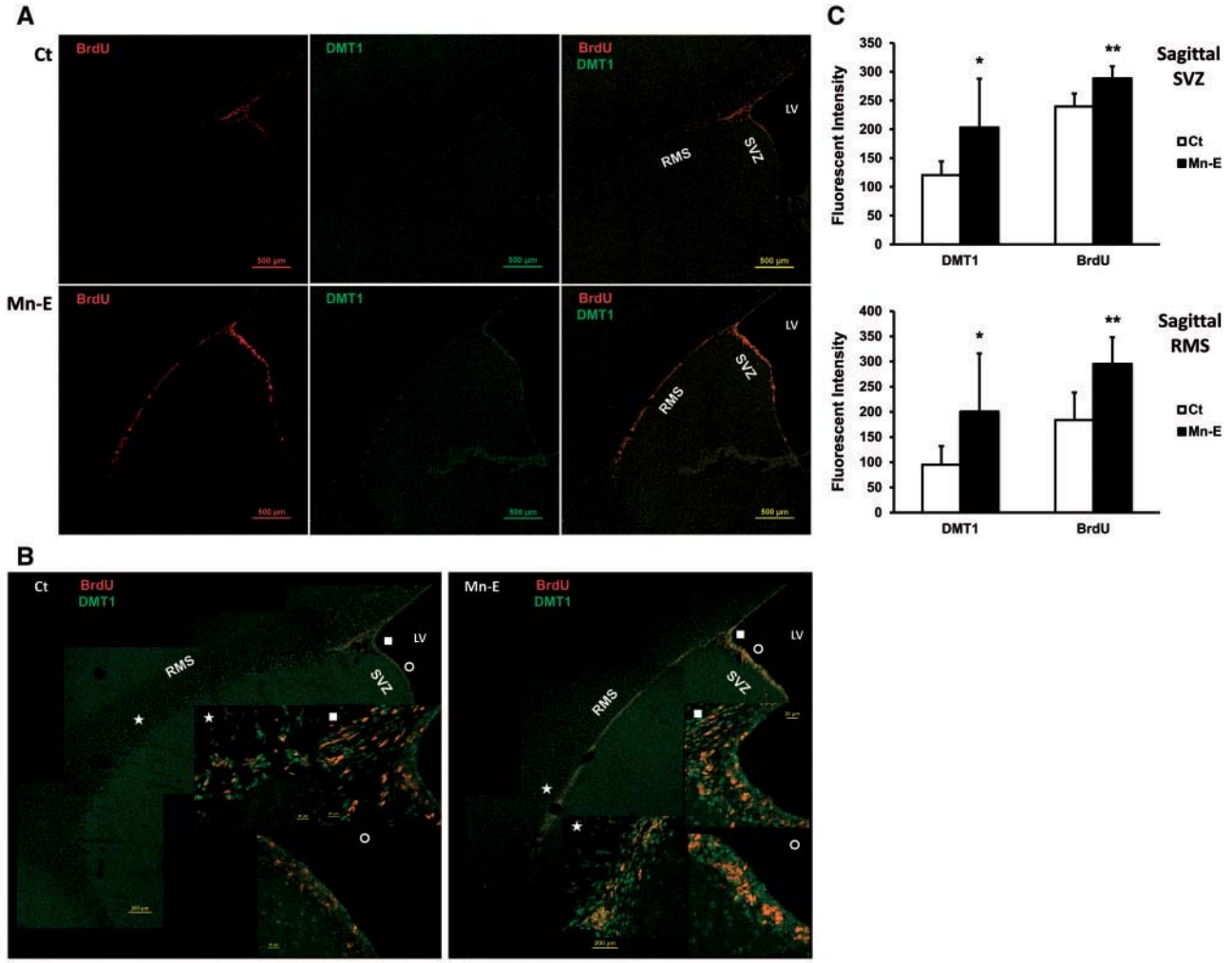

FIG. 2. IHC double-staining of BrdU and DMT1 in SVZ and RMS by sagittal sections. A, Typical sagittal images at low magnification (×40) from control and Mn-exposed animals stained for BrdU (red) and DMT1 (green). B, Typical sagittal images with high magnifications (×100 or × 600). The symbols of white square/circle and white star represent the regions approximating SVZ and RMS, respectively, which were used to "zoom-in" the confocal images with ×600 in magnification. Confocal data on sagittal sections from additional animals in the same experiments ($n = 3$) are presented in Supplementary Figure 2. C, Fluorescent intensity quantification data of DMT1 and BrdU. Data represent mean ± SD, $n = 3$; $^{*}P < 0.05$, $^{**}P < 0.01$, when compared with the control. Ct, control group; Mn-E, Mn-exposed group.

region revealed that the DCX-labeled neuroblasts, which were generated from the SVZ, formed chains during their migration to the olfactory bulb via this astrocytic tube along the RMS (Supplementary Figs. S2A–C). From the sagittal sections, BrdU(+) cells were oriented along the RMS, triple-staining with BrdU, GFAP, and DCX revealed a similar spatial distribution pattern of GFAP- and DCX-labeled cells in the RMS (Figs. 4A and 4B). Images with higher magnifications in Figures 4C1, 4D1, and 4E1 further revealed that the green DCX fluorescent signals and blue GFAP fluorescent signals distributed around the BrdU-labeled nuclei. On these sagittal sections, Mn exposure significantly increased the proliferating cell numbers of BrdU-, GFAP-, and DCX-labeled cells (Figs. 4A, 4B, 4C2, 4D2, and 4E2).

Thus, the data from triple-staining of BrdU, GFAP, and DCX in both coronal and sagittal sections suggest that subchronic exposure to Mn induces the proliferation of both ASCs and neuroblasts in the SVZ as well as in the RMS, and the neuroblasts appeared to contribute to the majority of the proliferating cell population. Although most of the BrdU(+) proliferating cells appeared to be DCX(+) cells in the SVZ, it is highly possible that the type B astrocytic progenitor cells may be potentially a major proliferating population affected by Mn exposure. This is due to the fact that both transit amplifying type C progenitors and the type A neuroblasts are originally derived from type B astrocytic progenitors.

Dmt1 mRNA and Protein Expression Levels in the SVZ Following In Vivo Mn Exposure

To further confirm the IHC finding of increased expression in DMT1 following Mn exposure, we quantified the mRNA and protein expression of *Dmt1* in the SVZ tissue. By normalizing with the internal reference gene *Actb*, our results showed that the mRNA expression level of *Dmt1* was increased approximately 13% following *in vivo* Mn exposure, which was significantly higher than that of control ($P < 0.05$; Fig. 5A). The Western blot analyses further confirmed a significantly increased protein level of DMT1 in Mn-exposed SVZ tissues when compared with controls ($P < 0.01$) (Figs. 5B and 5C). These observations are in a good agreement with our previous finding that Mn exposure

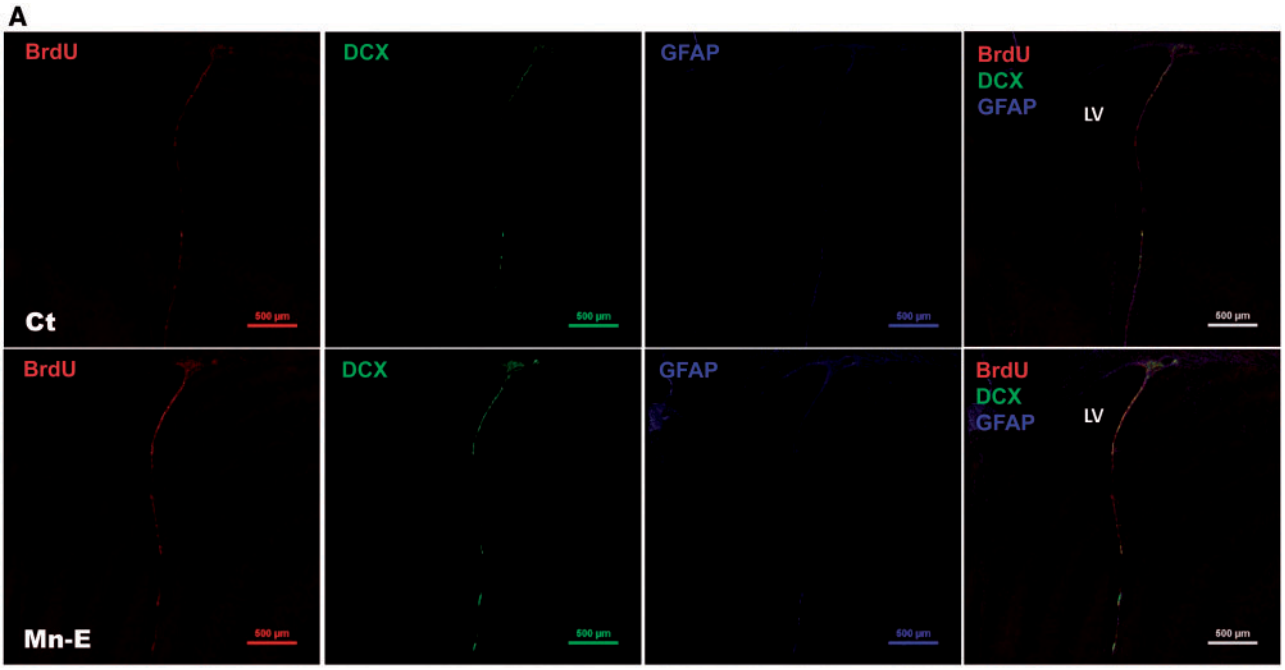

FIG. 3. IHC triple-staining of BrdU, GFAP, and DCX in the SVZ by coronal sections. A, Typical coronal images at low magnification (×40) from control and Mn-exposed animals ($n = 3$) stained for BrdU (red), DCX (green), and GFAP (blue). Images were taken sequentially using the same imaging parameters. B1, Typical images of control coronal section at high magnification (×200). The symbols of white square and circle represent the approximate regions used to "zoom-in" the confocal images. B2, Typical images of Mn-exposed coronal section at high magnification (×200). The symbols of white square and circle represent the approximate regions used to "zoom-in" the confocal images. C1, Control "zoom-in" images of the region labeled with the white square in Figure 3B1. White arrows point at the BrdU-labeled nuclei that are not surrounded by green DCX fluorescent signals. C2, Mn-exposed "zoom-in" images of the region labeled with the white square in Figure 3B2. White arrows point at the BrdU-labeled nuclei that are not surrounded by green DCX fluorescent signals. D1, Control "zoom-in" images of the region labeled with the white circle in Figure 3B1. D2, Mn-exposed "zoom-in" images of the region labeled with the white circle in Figure 3B2. White arrows point at the BrdU-labeled nuclei that are not surrounded by green DCX fluorescent signals. Ct, control group; Mn-E, Mn-exposed group.

up-regulates DMT1 expression in the choroid plexus (Wang *et al.*, 2006).

We also used double-staining of DMT1/GFAP in coronal sections to confirm the expression of DMT1 in GFAP(+) cells. Images in Supplementary Figure 3 displayed clear colocalization of GFAP and DMT1 in SVZ. Since the primary antibodies against DMT1 and DCX were produced from the same host (rabbit), the experiment was unable to repeat by double-staining of DMT1/DCX in neuroblasts.

Expression Levels of Gfap, Nestin, and Dcx mRNA in SVZ and Effect of In Vivo Mn Exposure

GFAP is highly expressed in proliferating type B cells. Nestin is a highly specific marker for transit amplifying progenitor type C cells, which are directly derived from ASCs in SVZ (Michalczyk and Ziman, 2005). To confirm the findings of the elevated adult neurogenesis following Mn exposure, the mRNA expression levels of *Gfap*, *Nestin*, and *Dcx* were quantified using qPCR. After normalizing with the internal reference gene *Actb*, our results showed about 256%, 31%, and 22% increases in *Gfap*, *Nestin*, and *Dcx* mRNA expression levels, respectively, following *in vivo* Mn exposure when compared with controls ($P < 0.05$; Figs. 6A–C). Interestingly, the increase in *Gfap* mRNA levels in the Mn-exposed SVZ tissues seemed to be conflicted with our IHC findings that the majority of BrdU(+) proliferating cells in the SVZ were DCX-stained type A neuroblasts. This could be due to the short duration of BrdU treatment, which labels the proliferating cells for only 5 days. By the time of IHC examination, a significant population of these BrdU(+)/GFAP(+) cells may have already turned into type C or type A cells, leaving limited GFAP(+) cells associated with BrdU. Regardless which cell types may be the primary target of Mn toxicity, these data provide the evidence that Mn exposure up-regulated the adult neurogenesis in SVZ. In addition, the ability to determine the expression of Nestin in collected tissues verifies that the SVZ dissection method used in the current study was effective.

DISCUSSION

Our previous studies using XRF microscopy combined with IHC demonstrate that Cu concentrations are several orders higher in the SVZ than in other brain regions (Pushkar *et al.*, 2013). The AAS data presented in the current study support a significant accumulation of Cu in the SVZ compared with other selected brain regions; furthermore, we demonstrate that *in vivo* Mn exposure apparently reduces Cu levels in the SVZ. Our IHC data reveal a significantly increased expression of BrdU(+) cells after Mn exposure, which are mainly accompanied with increased proliferating neuroblasts in the SVZ and RMS. Quantifying the expression of DMT1 in SVZ further shows that Mn exposure induces DMT1 expression in SVZ. More interestingly, qPCR quantitation of specific cellular markers for amplifying progenitor cells and neuroblasts confirms that *in vivo* Mn exposure up-regulates the adult neurogenesis in SVZ.

The current studies reveal a more abundant neurogenesis in both SVZ and RMS after *in vivo* Mn exposure. We have recently used the HPLC to quantify neurotransmitter levels in STR, substantia nigra, and HP in this rat model (ie, by i.p. injections of

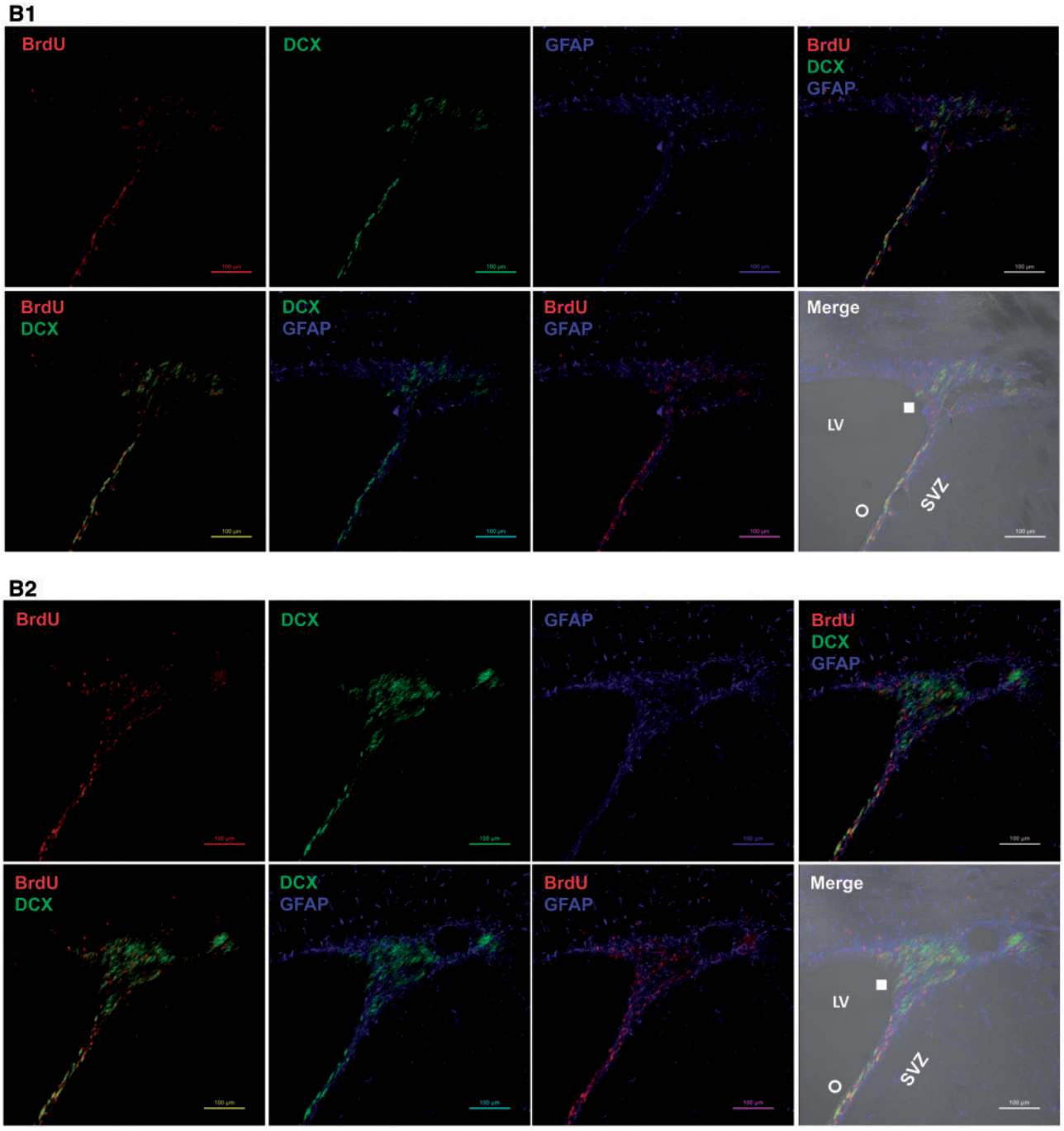

FIG. 3. Continued.

6 mg Mn/kg or 15 mg Mn/kg for 4 weeks). Mn exposure at 6 mg/kg does not cause significant changes in most neurochemical parameters examined except for 3,4-Dihydroxyphenylacetic acid (DOPAC) (about 30% increases). The dosing at 15 mg/kg, however, shows a significant alteration in striatum dopaminergic function (O'Neal *et al.*, 2014). Thus, it seems likely that a great accumulation of Mn in brain regions, such as STR, substantia nigra, and HP after subchronic Mn exposure at 6 mg/kg (Robison *et al.*, 2012; Zheng *et al.*, 2009) may cause subtle neuronal injuries. These subtle changes may trigger the neurogenesis process in the SVZ, leading to the proliferation and migration of DCX(+) neuroblasts along the RMS for repairing purpose. It is also possible that a naturally high Cu level in the SVZ is needed to secure the neurogenesis; yet a disrupted Cu level in the SVZ by Mn exposure may trigger the neurogenesis process, leading to an increased expression of BrdU(+) proliferating cells (discussed below). These hypotheses, however, will require extensive experimental proofs.

Previous works by this laboratory have established that Mn exposure induces the overexpression of DMT1 (Wang *et al.*, 2006). The current *in vivo* studies by both IHC and Western/qPCR quantifications substantiate this finding. The increased DMT1

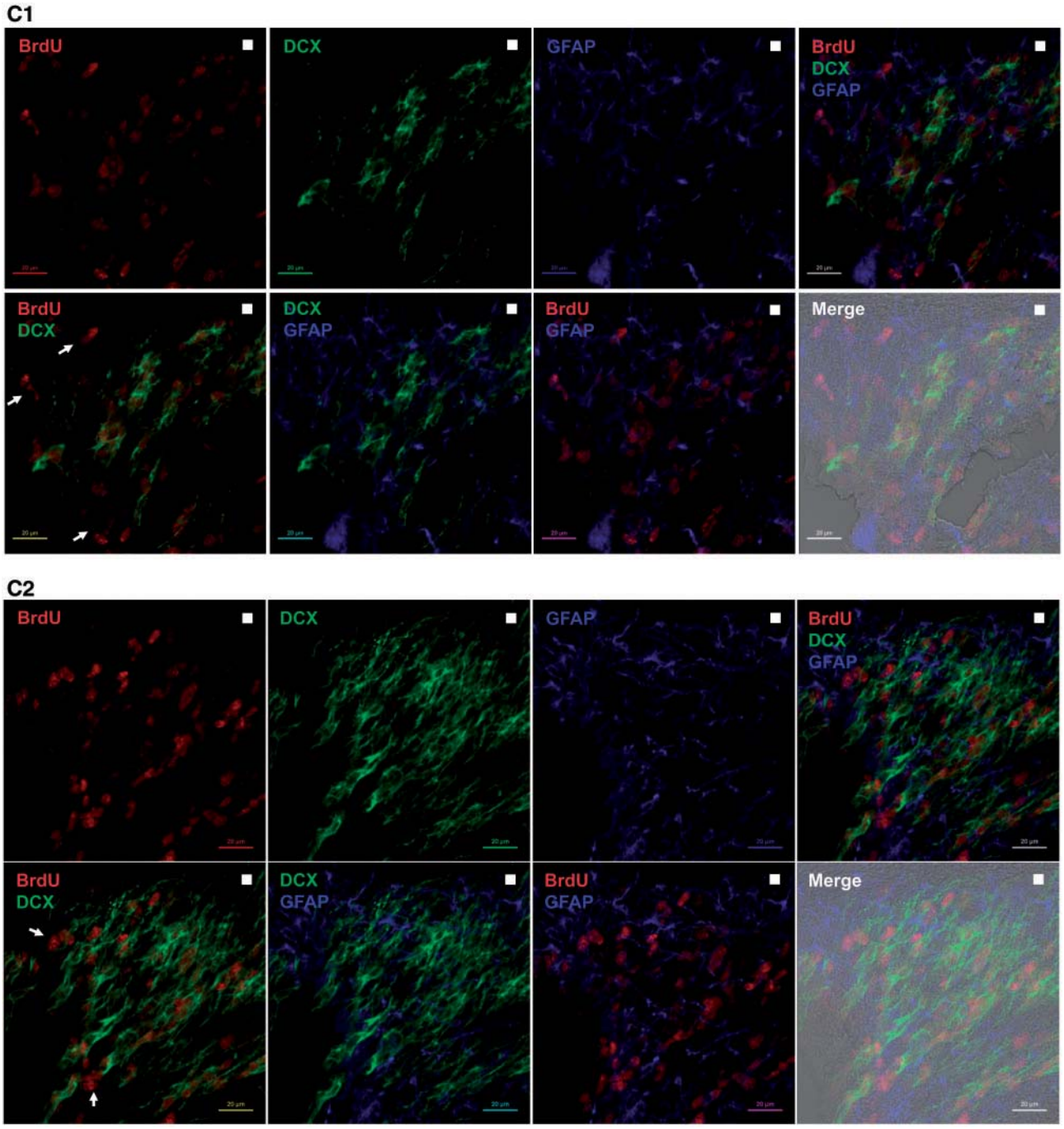

FIG. 3. Continued.

expression is due mainly to Mn replacement of Fe in [Fe-S] clusters of iron regulatory protein-1 (IRP1) whose conformational change facilitates the binding of IRP1 to mRNAs containing the stem-loop structure in their 3′-untranslated region, such as mRNAs encoding transferrin receptor (TfR) and DMT1 (Andrews, 1999; Klausner *et al.*, 1993; Li *et al.*, 2005; Wang *et al.*, 2006). Such a binding stabilizes protein expression, increases the cellular level of TfR and DMT1, and results in an increased metal uptake that is mediated by these metal transporters. This mechanism may explain the up-regulated expression of DMT1 in SVZ and RMS after Mn exposure and the ensuing increase in Mn uptake in these regions. Cellular Mn overload may in turn cause the disrupted Cu regulation.

Since DMT1 also mediates cellular uptake of Cu, it is logical to assume that increased DMT1 expression in SVZ and RMS would lead to an increased Cu uptake. However, our AAS data clearly demonstrate a reduced Cu level in the SVZ after *in vivo* subchronic Mn exposure. Thus, there must be a yet-undefined mechanism, other than DMT1, in the SVZ that respond to Mn treatment entirely different from other brain regions with regard to the regulation of cellular Cu status. Noticeably, cellular Cu levels are not solely regulated by DMT1; other transporters

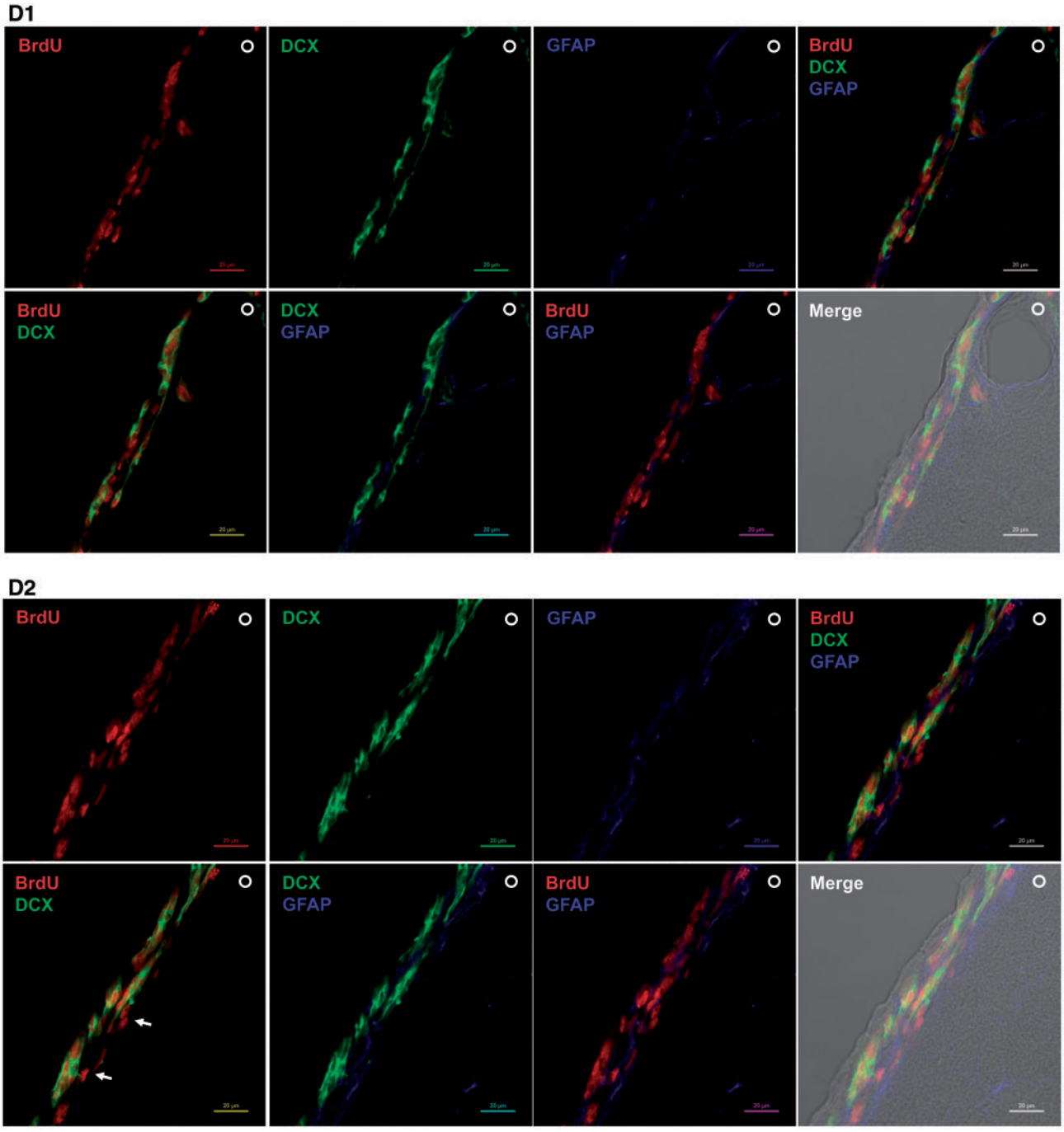

FIG. 3. Continued.

such as CTR1, ATP7A, and ATP7B, and the cytochrome oxidase enzyme complex (COX17) are involved in cellular Cu homeostasis (Zheng and Monnot, 2012). The interaction of Mn with these Cu transporters in the SVZ and RMS thus deserves further exploration.

Our observations raise several interesting research questions. First, what factors contribute to the high Cu level in the SVZ? A great buildup of any metals in a particular region could be the result of (1) increased metal uptake by a particular cell type, (2) decreased metal release by the hosting cells, and/or (3) increased intracellular binding. Currently little is known about Cu transporters mediating cellular Cu uptake or release in the SVZ and the intracellular ligands that withhold the high amount of Cu ions. Unlike Mn-induced Cu accumulation in other brain regions, Mn accumulation in the SVZ, owing to the increased DMT1 expression, leads to a reduced Cu level; the latter is certainly not mediated by DMT1. Thus, the complexity regarding Cu regulatory mechanisms in this region appears to be a promising research subject for future exploration.

Second, what is the role of high Cu in the SVZ with regards to neurogenesis? Is there a threshold Cu level above or below which Mn exposure may trigger the proliferation,

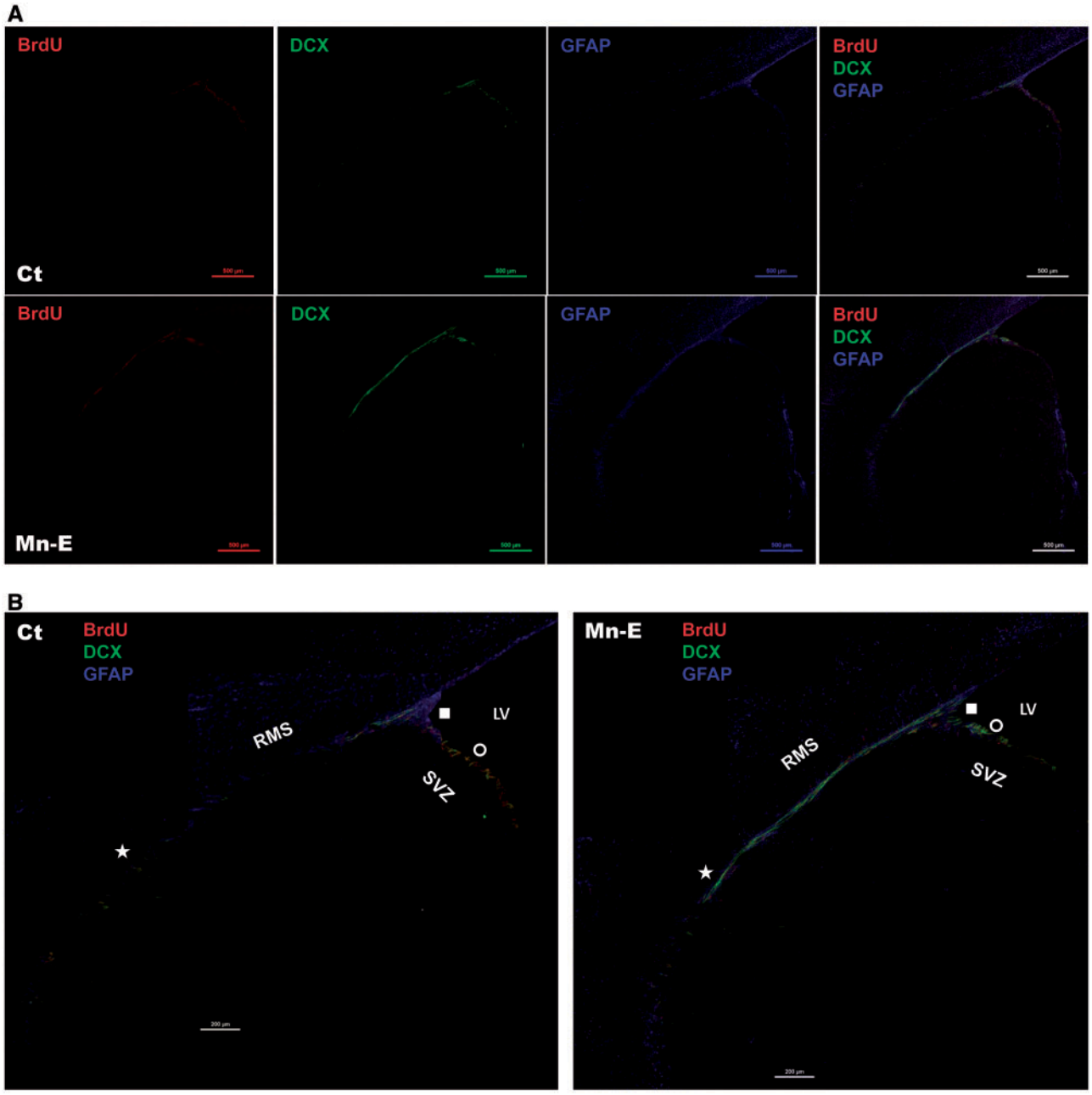

FIG. 4. IHC triple-staining of BrdU, GFAP, and DCX in the SVZ by sagittal sections. A, Typical sagittal images at low magnification (×40) from control and Mn-exposed animals ($n = 3$) stained for BrdU (red), DCX (green), and GFAP (blue). Images were taken sequentially using the same imaging parameters. B, Typical sagittal images at ×100 magnification from control and Mn-exposed animals stained for BrdU (red), DCX (green), and GFAP (blue). The symbols of white square, circle, and star represent the approximate regions used to "zoom-in" the confocal images. C1, Control "zoom-in" images of the region labeled with the white square in Figure 4B (Ct). White arrows point at the BrdU-labeled nuclei that are not surrounded by green DCX fluorescent signals. C2, Mn-exposed "zoom-in" images of the region labeled with the white square in Figure 4B (Mn-E). White arrows point at the BrdU-labeled nuclei that are not surrounded by green DCX fluorescent signals. D1, Control "zoom-in" images of the region labeled with the white circle in Figure 4B (Ct). White arrows point at the BrdU-labeled nuclei that are not surrounded by green DCX fluorescent signals. D2, Mn-exposed "zoom-in" images of the region labeled with the white circle in Figure 4B (Mn-E). The white arrows point at the BrdU-labeled nuclei that are not surrounded by green DCX fluorescent signals. E1, Control "zoom-in" images of the region labeled with the white star in Figure 4B (Ct). White arrows point at the BrdU-labeled nuclei that are not surrounded by green DCX fluorescent signals. E2, Mn-exposed "zoom-in" images of the region labeled with the white star in Figure 4B (Mn-E). The white arrows point at the BrdU-labeled nuclei that are not surrounded by green DCX fluorescent signals. Ct, control group; Mn-E, Mn-exposed group.

differentiation, and migration of neural stem/progenitor cells in SVZ and RMS? A reduced Cu level in the SVZ as a result of Mn exposure appears to suggest that a high Cu level may be necessary to restrain or stabilize the proliferation of BrdU(+) cells. Our current data showed a markedly increased expression of DCX(+) neuroblasts along with increased BrdU expression after Mn exposure. A recent x-ray study in this laboratory has observed that the Cu ions are primarily accumulated in the GFAP(+) type B cells, and Cu signals do not appear in the areas occupied by actively dividing cells (Pushkar *et al.*, 2013).

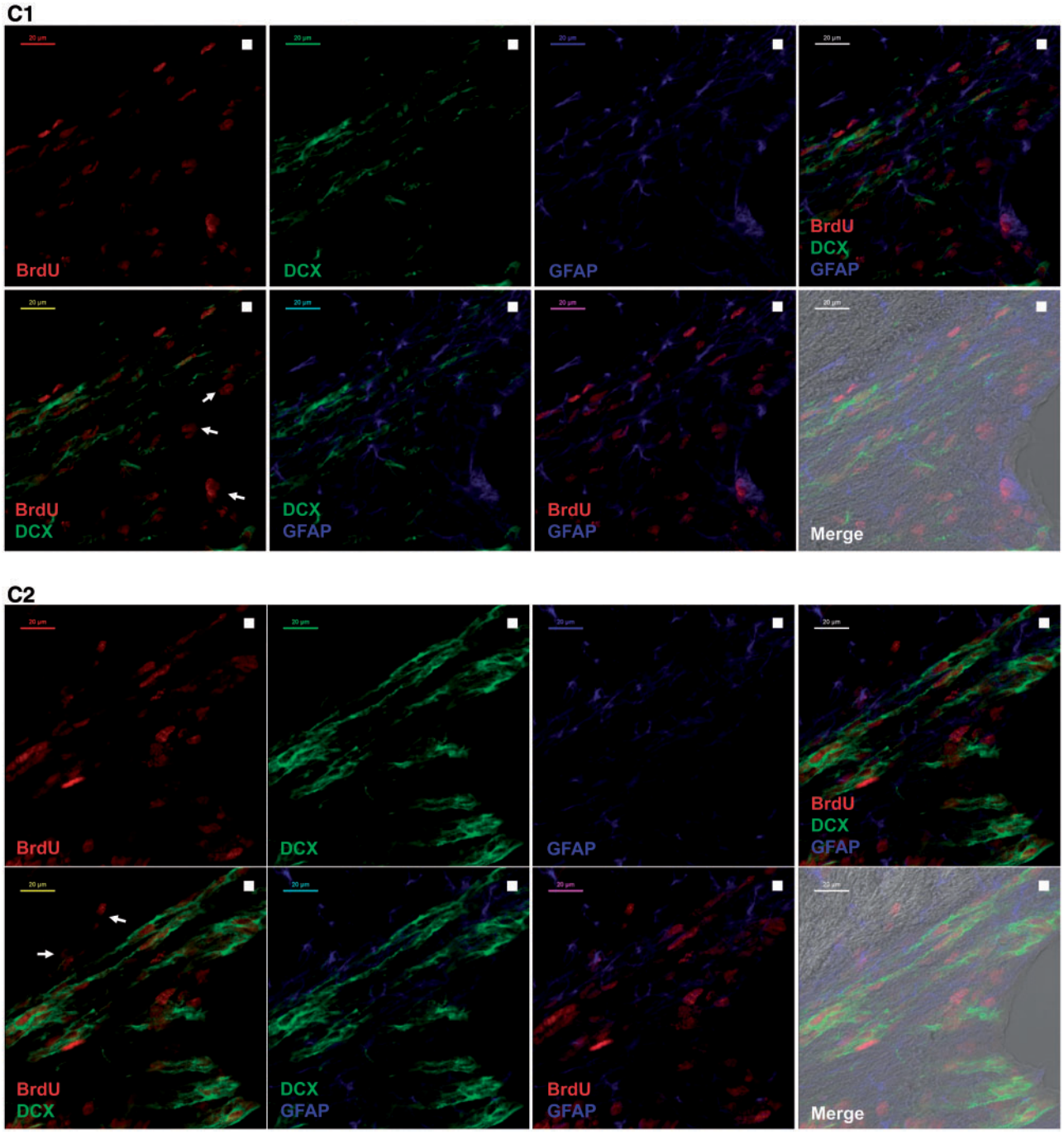

FIG. 4. Continued.

Existing data in literature have established that type A neuroblasts and type C transit progenitor cells are derived from type B ASCs; the latter are much slower in the rate of proliferation, but are the sources of type A and C cells (Doetsch *et al.*, 1997, 1999; Luskin, 1993; Menezes *et al.*, 1995). Our recent *in vitro* studies have shown a significant reduction of Cu accumulation in primary cultures of type B ASC cells after Mn exposure (data not shown). It is quite possible that a disruption of the high cellular Cu status in ASCs by Mn exposure may trigger type B cells to proliferate and differentiate, leading to the overwhelming expression of DCX(+) neuroblasts in the SVZ and RMS. The increased DCX(+) neuroblast population, on the other hand, may contribute to the significant elevation of DMT1 expression level in the SVZ and RMS. Thus, it is reasonable to speculate that the triggered neurogenesis may take place mainly in GFAP(+) ASCs, particularly considering the fact that *in vivo* Mn exposure also increases *Gfap* and *Nestin* mRNA expressions in the SVZ. Nestin is a unique marker for dividing neural precursor cells in SVZ and subgranular zone. Once cells are differentiated, nestin is replaced by more generic marker GFAP (Michalczyk

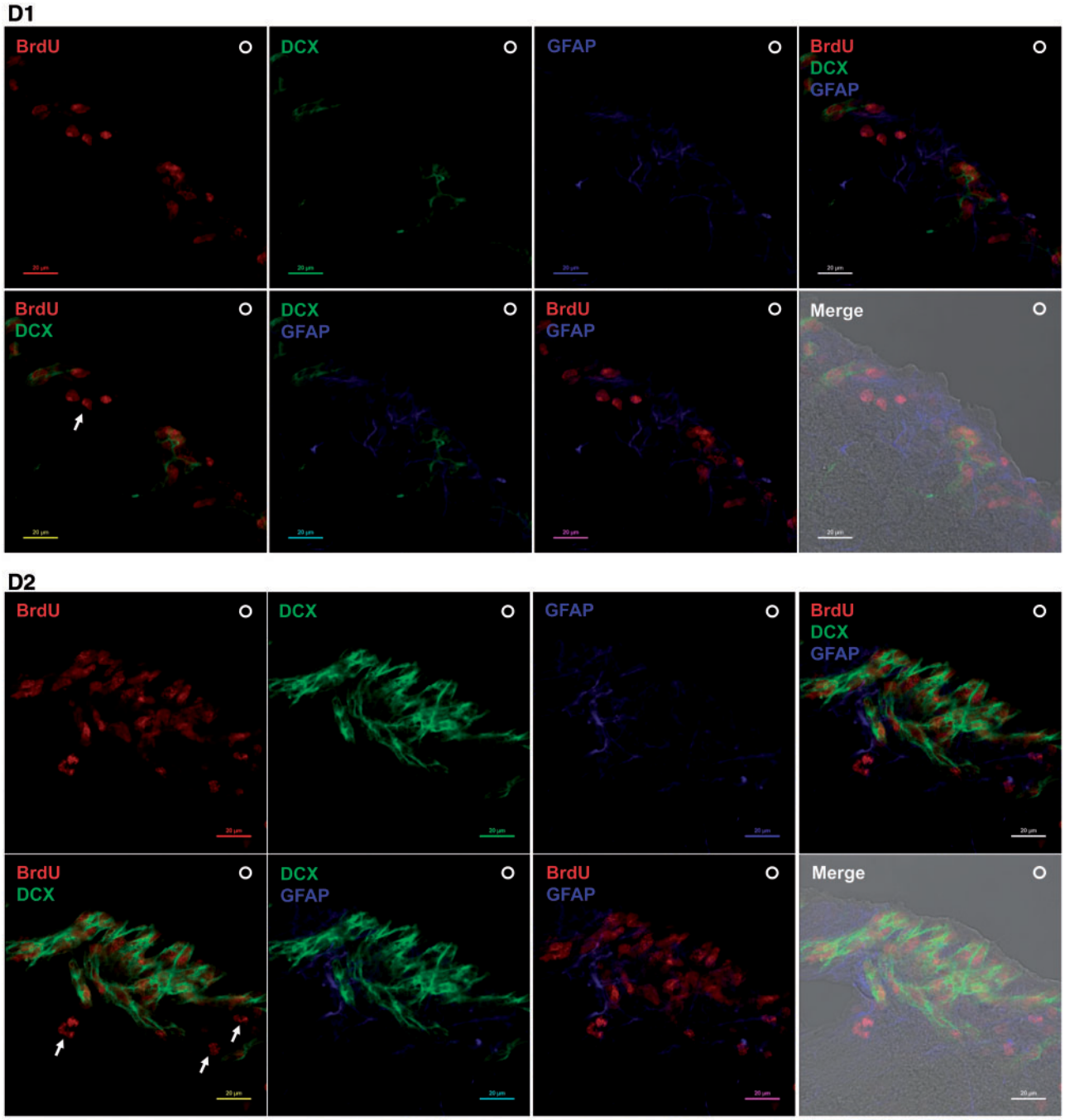

FIG. 4. Continued.

and Ziman, 2005). It will be highly interesting to explore the threshold level of Cu in a particular cell type in SVZ that is responsible for initiation of neurogenesis.

Finally, what are the consequences of activated neurogenesis? Where is the ultimate destination of the newly derived progenitor cells, toward solely to the olfactory bulb or also distributed to injured brain regions such as striatum, substantia nigra, or HP, the regions known to be affected by Mn intoxication? Clearly, the efforts in understanding these questions may lead to the discovery of novel therapeutic means for treatment of neurodegenerative disorders.

Our studies have the following limitations. As indicated above, cellular Cu status is regulated by multiple metal transporters. Our current study focuses only on DMT1. Although this study indeed provides valuable information on DMT1 in the SVZ and RMS, it cannot exclude the impact of other metal transporters, particularly those directly participating in Cu uptake, storage, and release. We are currently working on these transporters in the SVZ and RMS. Additionally, our previous work has shown that among the cerebral capillary, choroid plexus, brain parenchyma, and CSF, the choroid plexus tissue exhibits the highest capacity in acquiring Cu from the blood circulation

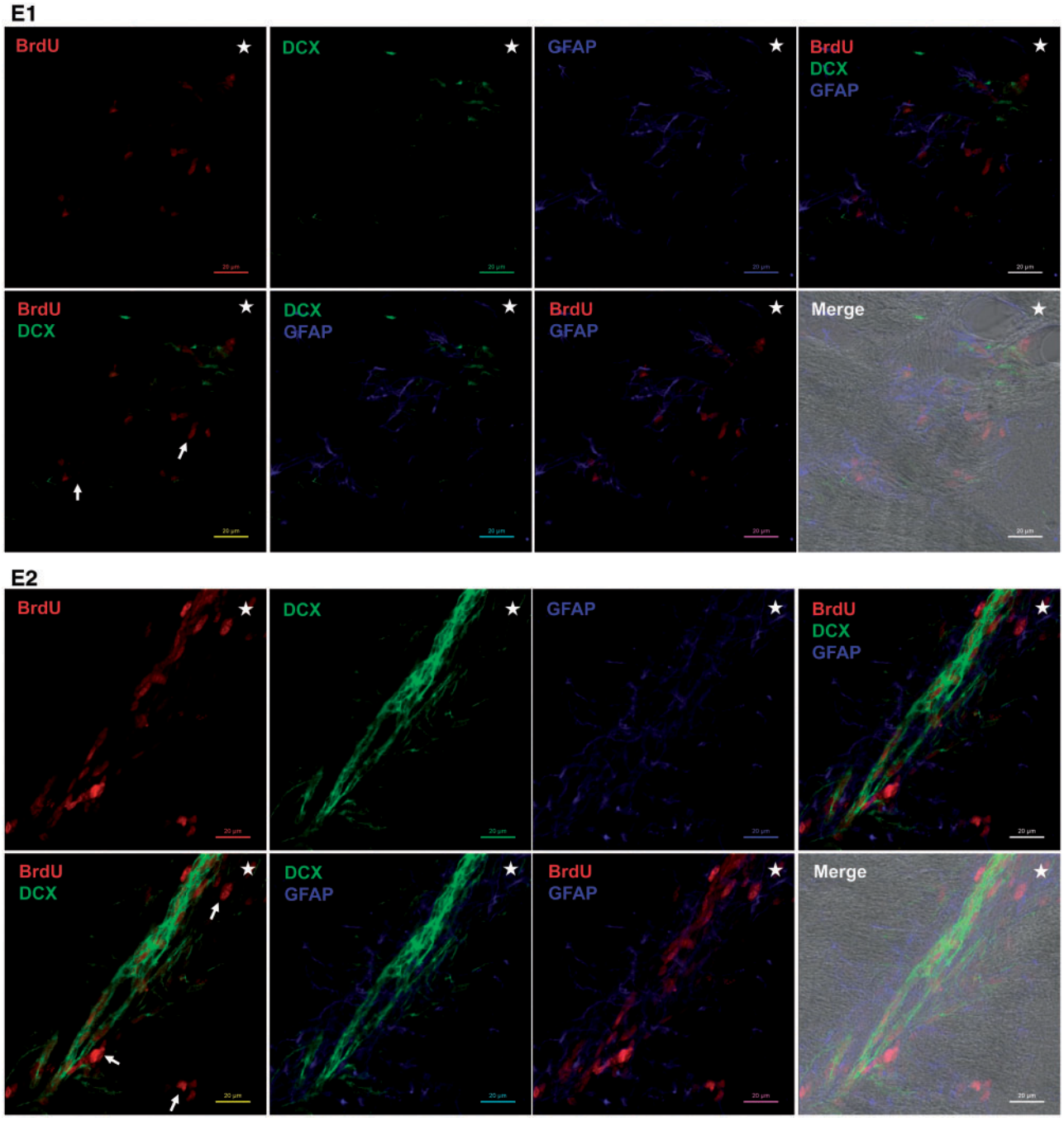

FIG. 4. Continued.

irrespective to what Cu species is used (Choi and Zheng, 2009). As the choroid plexus is immediately adjacent to the SVZ, the tissue may have significant impact on how Cu is regulated by the SVZ. The current study did not address this issue.

Another limitation is that with the current data, it remains uncertain if the changes in fluorescent markers in the SVZ and RMS represent a true increase in neurogenesis or some other alterations in the biological process secondary to Mn toxicity, eg, an inhibited migration, a compensatory effect due to Mn-induced cellular loss, or the oxidative stress taking place in the SVZ. Understandably, a thorough investigation to explore the direct evidence of Mn-induced neurogenesis in SVZ is desirable.

In conclusion, the data presented in this study demonstrate that Cu concentrations are higher in the SVZ than in other brain regions. Subchronic Mn exposure *in vivo* appears to increase fluorescent signals associated with neurogenesis in SVZ, which correlates to increased expressions of ASCs and neuroblasts. Mn-induced DMT1 expression in SVZ and RMS is evident; it may partly contribute to cellular overload of Mn in SVZ. Future in-depth mechanistic investigations to understand the dose-time-response relationship between Mn exposure and neurogenesis

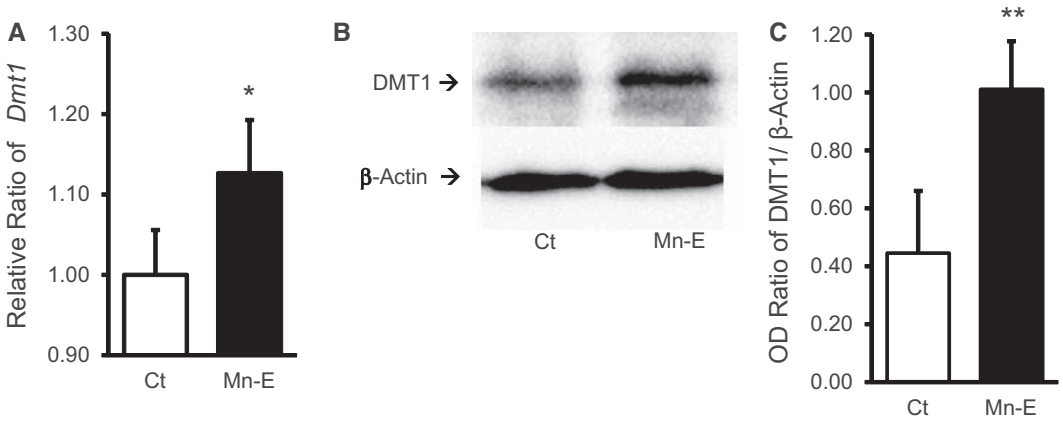

FIG. 5. mRNA and protein expression of DMT1 in control and Mn-exposed SVZ tissues. A, mRNA expression level of *Dmt1* in control and Mn-exposed SVZ tissues was quantified by qPCR and expressed as the relative expression ratio by normalizing with the *Actb*. The data are representative of triplicate experiments. Data represent mean ± SD, $n = 4–5$; $^{*}P < 0.05$, when compared with controls. B, Typical Western blot autographs of DMT1 in SVZ tissues from 3 control and 3 Mn-exposed animals. C, Quantification of Western blot densitometry and statistical analysis. Ct, control group; Mn-E, Mn-exposed group. Data represent mean ± SD, $n = 3$; $^{**}P < 0.01$, when compared with controls.

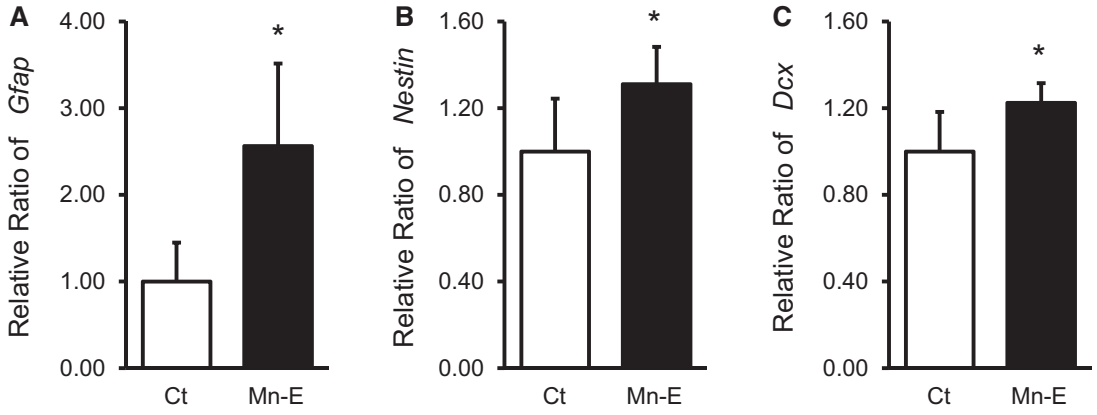

FIG. 6. *Gfap*, *Nestin*, and *Dcx* mRNA expression in control and Mn-exposed SVZ tissues. A, mRNA expression levels of *Gfap* in control and Mn-exposed SVZ tissues were measured using qPCR and expressed as the relative expression ratio by normalizing with the *Actb*. B, mRNA expression levels of *Nestin* in control and Mn-exposed SVZ tissues were quantified by qPCR and expressed as the relative expression ratio by normalizing with the *Actb*. C, mRNA expression levels of *Dcx* in control and Mn-exposed SVZ tissues were quantified by qPCR and expressed as the relative expression ratio by normalizing with the *Actb*. The data are representative of triplicate experiments. Data represent mean ± SD, $n = 5–6$; $^{*}P < 0.05$, when compared with controls. Ct, control group; Mn-E, Mn-exposed group.

in SVZ and RMS as well as the role of Cu in adult neurogenesis are well warranted. The research in this direction will likely create a new productive avenue in Mn neurotoxicity research.

SUPPLEMENTARY DATA

Supplementary data are available online at http://toxsci.oxfordjournals.org/.

FUNDING

NIH/National Institute of Environmental Health Sciences Grants Number R01 ES008146-14.

REFERENCES

Andrews, N. C. (1999). The iron transporter DMT1. *Int. J. Biochem. Cell Biol.* **31,** 991–994.

Barnham, K. J., and Bush, A. I. (2008). Metals in Alzheimer's and Parkinson's diseases. *Curr. Opin. Chem. Biol.* **12,** 222–228.

Burdo, J. R., Menzies, S. L., Simpson, I. A., Garrick, L. M., Garrick, M. D., Dolan, K. G., Haile, D. J., Beard, J. L., and Connor, J. R. (2001). Distribution of divalent metal transporter 1 and metal transport protein 1 in the normal and Belgrade rat. *J. Neurosci.* **66,** 1198–1207.

Choi, B. S., and Zheng, W. (2009). Copper transport to the brain by the blood-brain barrier and blood-CSF barrier. *Brain Res.* **1248,** 14–21.

Curtis, M. A., Faull, R. L. M., and Eriksson, P. S. (2007). The effect of neurodegenerative diseases on the subventricular zone. *Nat. Rev. Neurosci.* **8,** 712–723.

Deibel, M. A., Ehmann, W. D., and Markesbery, W. R. (1996). Copper, iron, and zinc imbalances in severely degenerated brain regions in Alzheimer's disease: possible relation to oxidative stress. *J. Neurol. Sci.* **143,** 137–142.

Doetsch, F., Caillé, I., Lim, D. A., García-Verdugo, J. M., and Alvarez-Buylla, A. (1999). Subventricular zone astrocytes are

neural stem cells in the adult mammalian brain. *Cell* **97,** 703–716.

Doetsch, F., Garcia-Verdugo, J. M., and Alvarez-Buylla, A. (1997). Cellular composition and three-dimensional organization of the subventricular geminal zone in the adult mammalian brain. *J. Neurosci.* **17,** 5046–5061.

El Meskini, R., Crabtree, K. L., Cline, L. B., Mains, R. E., Eipper, B. A., and Ronnett, G. V. (2007). ATP7A (Menkes protein) functions in axonal targeting and synaptogenesis. *Mol. Cell Neurosci.* **34,** 409–421.

Fu, X., Zhang, Y., Jiang, W., Monnot, A. D., Bates, C. A., and Zheng, W. (2014). Regulation of copper transport crossing brain barrier systems by Cu-ATPases: effect of manganese exposure. *Toxicol Sci.* **139,** 432–451.

Gaggelli, E., Kozlowski, H., Valensin, D., and Valensin, G. (2006). Copper homeostasis and neurodegenerative disorders (Alzheimer's, prion, and Parkinson's diseases and amyotrophic lateral sclerosis). *Chem. Rev.* **106,** 1995–2044.

Ghashghaei, H. T., Lai, C., and Anton, E. S. (2007). Neuronal migration in the adult brain: are we there yet? *Nat. Rev. Neurosci.* **8,** 141–151.

Gruenheid, S., Cellier, M., Vidal, S., and Gros, P. (1995). Identification and characterization of a second mouse Nramp gene. *Genomics* **25,** 514–525.

Gunshin, H., Mackenzie, B., Berger, U. V., Gunshin, Y., Romero, M. F., Boron, W. F., Nussberger, S., Gollan, J. L., and Hediger, M. A. (1997). Cloning and characterization of a mammalian proton-coupled metal-ion transporter. *Nature* **388,** 482–488.

Haremaki, T., Fraser, S. T., Kuo, Y. M., Baron, M. H., and Weinstein, D. C. (2007). Vertebrate Ctr1 coordinates morphogenesis and progenitor cell fate and regulates embryonic stem cell differentiation. *Proc. Natl Acad. Sci. U. S. A.* **104,** 12029–12034.

Harris, E. D. (2001). Copper homeostasis: the role of cellular transporters. *Nutr. Rev.* **59**, 281–285.

Imura, T., Nakano, I., Kornblum, H. I., and Sofroniew, M. V. (2006). Phenotypic and functional heterogeneity of GFAP-expressing cells in vitro: differential expression of LeX/CD15 by GFAP-expressing multipotent neural stem cells and non-neurogenic astrocytes. *Glia* **53,** 277–293.

Joseph, R. P., Bruce, B. (2001). Dietary copper deficiency alters protein levels of rat dopamine β-monooxygenase and tyrosine monooxygenase. *Exp. Biol. Med.* **226,** 199–207.

Klausner, R. D., Rouault, T. A., and Harford, J. B. (1993). Regulating the fate of mRNA: the control of cellular iron metabolism. *Cell* **72**, 19–28.

Li, G. J., Zhao, Q., and Zheng, W. (2005). Alteration at translational but not transcriptional level of transferrin receptor expression following manganese exposure at the blood-CSF barrier in vitro. *Toxicol. Appl. Pharmacol.* **205,** 188–200.

Lledo, P. M., Alonso, M., and Grubb, M. S. (2006). Adult neurogenesis and functional plasticity in neuronal circuits. *Nat. Rev. Neurosci.* **7,** 179–193.

Lois, C., Garcia-Verdugo, J. M., and Alvarez-Buylla, A. (1996). Chain migration of neuronal precursors. *Science* **271,** 978–981.

Lorraine, G., Christine, K., and Harry, J. M. (2011). Iron and copper in fetal development. *Semin. Cell Dev. Biol.* **22,** 637–644.

Luskin, M. B. (1993). Restricted proliferation and migration of postnatally generated neurons derived from the forebrain subventricular zone. *Neuron* **11,** 173–189.

Martino, G., and Pluchino, S. (2006). The therapeutic potential of neural stem cells. *Nat. Rev. Neurosci.* **7,** 395–406.

Matés, J. M., Segura, J. A., Alonso, F. J., and Márquez, J. (2010). Roles of dioxins and heavy metals in cancer and neurological diseases using ROS-mediated mechanisms. *Free Radic. Biol. Med.* **49,** 1328–1341.

Matusch, A., Depboylu, C., Palm, C., Wu, B., Höglinger, G. U., Schäfer, M. K., and Becker, J. S. (2010). Cerebral bioimaging of Cu, Fe, Zn, and Mn in the MPTP mouse model of Parkinson's disease using laser ablation inductively coupled plasma mass spectrometry (LA-ICP-MS). *J. Am. Soc. Mass Spectrom.* **21,** 161–171.

Menezes, J. R., Smith, C. M., Nelson, K. C., and Luskin, M. B. (1995). The division of neuronal progenitor cells during migration in the neuonatal mammalian forebrain. *Mol. Cell. Neurosci.* **6,** 496–508.

Michalczyk, K., and Ziman, M. (2005). Nestin structure and predicted function in cellular cytoskeletal organisation. *Histol. Histopathol.* **20,** 665–671.

Monnot, A. D., Zheng, G., and Zheng, W. (2012). Mechanism of copper transport at the blood-cerebrospinal fluid barrier: influence of iron deficiency. *Exp. Biol. Med.* **237,** 327–333.

Niciu, M. J., Ma, X. M., El Meskini, R., Pachter, J. S., Mains, R. E., and Eipper, B. A. (2007). Altered ATP7A expression and other compensatory responses in a murine model of Menkes disease. *Neurobiol. Dis.* **27,** 278–291.

O'Neal, S. L., Lee, J. W., Zheng, W., and Cannon, J. R. (2014). Subchronic manganese exposure in rats is a neurochemical model of early manganese toxicity. *Neurotoxicology* **44,** 303–313.

Pushie, M. J., Pickering, I. J., Martin, G. R., Tsutsui, S., Jirik, F. R., and George, G. N. (2011). Prion protein expression level alters regional copper, iron and zinc content in the mouse brain. *Metallomics* **3,** 206–214.

Pushkar, Y., Robison, G., Sullivan, B., Fu, S. X., Kohne, M., Jiang, W., Rohr, S., Lai, B., Marcus, M. A., Zakharova, T., *et al.* (2013). Aging results in copper accumulations in glial fibrillary acidic protein-positive cells in the subventricular zone. *Aging Cell* **12,** 823–832.

Robison, G., Zakharova, T., Fu, X., Jiang, W., Fulper, R., Barrea, R., Marcus, M. A., Zheng, W., and Pushkar, Y. (2012). X-ray fluorescence imaging: a new tool for studying manganese neurotoxicity. *PLoS One* **7,** e48899.

Skjorringe, T., Moller, L., and Moos, T. (2012). Impairment of interrelated iron- and copper homeostatic mechanisms in brain contributes to the pathogenesis of neurodegenerative disorders. *Front. Pharmacol.* **3,** 169.

Takahashi, Y., Kako, K., Kashiwabara, S., Takehara, A., Inada, Y., Arai, H., Nakada, K., Kodama, H., Hayashi, J., Baba, T., *et al.* (2002). Mammalian copper chaperone cox17p has an essential role in activation of cytochrome C oxidase and embryonic development. *Mol. Cell Biol.* **22,** 7614–7621.

Turski, M. L., and Thiele, D. J. (2009). New roles for copper metabolism in cell proliferation, signaling, and disease. *J. Biol. Chem.* **284,** 717–721.

Uriu-Adams, J., Scherr, R., Lanoue, L., and Keen, C. L. (2010). Influence of copper on early development: prenatal and postnatal considerations. *Biofactors* **36,** 136–152.

Wang, L., Ohishi, T., Shiraki, A., Morita, R., Akane, H., Ikarashi, Y., Mitsumori, K., and Shibutani, M. (2012). Developmental exposure to manganese chloride induces sustained aberration of neurogenesis in the hippocampal dentate gyrus of mice. *Toxicol. Sci.* **127**, 508–521.

Wang, X., Li, G. J., and Zheng, W. (2006). Up-regulation of DMT1 expression in choroidal epithelial cells following manganese exposure. *Brain Res.* **1097,** 1–10.

Zheng, W., Jiang, Y. M., Zhang, Y., Jiang, W., Wang, X., and Cowan, D. M. (2009). Chelation therapy of manganese intoxication with para-aminosalicylic acid (PAS) in Sprague-Dawley rats. *Neurotoxicology* **30,** 240–248.

Zheng, W., and Monnot, A. D. (2012). Regulation of brain iron and copper homeostasis by brain barrier systems: implication in neurodegenerative diseases. *Pharmacol. Ther.* **133,** 177–188.

Zheng, W., Ren, S., and Graziano, J. H. (1998). Manganese inhibits mitochondrial aconitase: a mechanism of manganese neurotoxicity. *Brain Res.* **799,** 334–342.

Zheng, W., Zhao, Q., Slavkovich, V., Aschner, M., and Graziano, J. H. (1999). Alteration of iron homeostasis following chronic exposure to manganese in rats. *Brain Res.* **833,** 125–132.